Performance of Nanoliter-Sized Droplet-based Microfluidic PCR

Fang Wang[a] and **Mark A. Burns**[*,a,b]

[a]Department of Chemical Engineering, University of Michigan, Ann Arbor, MI 48109

[b]Department of Biomedical Engineering, University of Michigan, Ann Arbor, MI 48109

Abstract

A microfluidic device was used to characterize PCR in aqueous-in-oil droplets for potential point-of-care applications. Droplets with a volume range of 5–250nL can be formed on-chip reproducibly, and PCR in the droplets shows amplification efficiencies comparable to benchtop reactions with no evaporation loss. A higher polymerase concentration is required in the reaction droplet while the optimal Magnesium ion concentration is the same for both on-chip and benchtop systems. The optimal hold time is 9 and 30 seconds for denaturation and annealing/extension in thermal cycling, respectively. With the optimized cycling parameters, the total reaction time is reduced to half of that required for benchtop PCR. For the droplets containing the same quantity of template DNA, the PCR yield is approximately the same with either fixed droplet size or fixed template DNA concentration. The droplet-based PCR can be monitored in real time with FRET probes, and provide amplification with a cycle threshold of ~10 cycles earlier than the benchtop instruments.

Keywords

Real-time PCR; Droplet; Microfluidics; Microdevice

1 Introduction

In recent years, droplet-based multiphase microfluidics has been emerging as a promising approach for fundamental and applied research in chemical and biological analyses. Droplet formation with sizes from femto- to microliter in a microfluidic system can be well controlled by adjusting the channel geometry and fluid flow rates (*e.g.*, T-junction (Garstecki et al. 2006; Nisisako et al. 2002; Thorsen et al. 2001) as well as flow focusing (Anna et al. 2003; Yobas et al. 2006)), or using electrohydrodynamic (EHD) methods such as dielectrophoresis (DEP) (Ahmed and Jones 2006; Jones 2001) and electrowetting on dielectric (EWOD) (Cho et al. 2003; Pollack et al. 2000, 2002). Other techniques for generating and actuating droplets using microfabricated pneumatic chopper (Chen and Lee 2006; Hsiung et al. 2006), surface acoustic wave (SAW) (Guttenberg et al. 2005), and electromagnetic force (Lehmann et al. 2006; Pipper et al. 2007) have also been reported. In addition, droplet manipulations including breakup (Link et al. 2004; Ting et al. 2006), fusion (Hung et al. 2006; Niu et al. 2008; Sarrazin et al. 2007; Yang et al. 2001; Um and Park 2009), mixing (Bringer et al. 2004; Sarrazin et al. 2007; Song et al. 2003) and sorting (Link et al. 2006; Tan et al. 2004) have been studied to further exploit the droplet-based microsystems. With the development of techniques for droplet generation and manipulation, droplet-based microfluidics offers the capability to form and isolate controllable reaction volumes, achieve rapid mixing of reagents, and increase the reaction throughput. Droplet-

[*]maburns@umich.edu; Fax: (734) 763 0459; Phone: (734) 764 4315.

based microsystems have been developed to perform a variety of chemical and biological reactions and analytical processes, such as nanoparticle synthesis (Chan et al. 2005; Hung et al. 2006; Shestopalov et al. 2004;), biological fluids analysis (Srinivasan et al. 2004), cell analysis (Chabert and Viovy 2008; He et al. 2005; Kumaresan et al. 2008), protein expression (Dittrich et al. 2005; Huebner et al. 2007) and crystallization (Zheng et al. 2004), and genetic analysis (Beer et al. 2007, 2008; Chabert et al. 2006; Guttenberg et al. 2005; Kumaresan et al. 2008; Lehmann et al. 2006; Mohr et al. 2007; Ohashi et al. 2007; Pipper et al. 2007; Srisa-Art et al. 2007).

As one crucial technique in most genetic analyses, the polymerase chain reaction (PCR) has been extensively investigated in miniaturized single-phase system, in order to achieve rapid and inexpensive analyses (Burns 2002). Droplet-based PCR not only offers the capability of reducing the reactor volume, but also provides the potential to alleviate the problems commonly found in single-phase PCR microsystems, such as evaporation loss and non-specific surface adsorption. In a single-phase PCR microsystem without any sealing components, evaporation loss could be 40% to 100% of the reaction volume (Wang et al. 2008). Using sealing agents reduces the evaporation, but increases the fabrication and operation complexity. Most reported on-chip droplet-based PCR were performed in monodisperse picoliter droplets (Beer et al. 2007, 2008). These systems have shown the ability to detect a single copy of nucleic acid molecule in a complex background, indicating applications such as detection of low concentrations of disease-associated mutations. Moreover, such a small droplet size (*i.e.*, reactor volume) significantly decreases the diffusion distance and thereby reduces the total reaction time, allowing earlier detection of target molecules in high-throughput.

A potential problem in picoliter droplet-based PCR is that the possible nonuniform encapsulation of template molecules (especially long templates) and reagents could lead to nonuniform amplification in monodisperse droplets. However, a statistical analysis of the amplified targets should be able to circumvent this problem as long as the droplet density and spacing are appropriate. Another problem with amplification in picoliter-sized droplets is that, for cases where downstream processes (e.g., restriction digestion, and hybridization) need to be performed, sufficient product molecules may not be available. In addition, in many PCR-based diagnoses, the initial target molecule concentrations in patient samples are so low that analysis in picoliter-sized droplets is not possible. For example, in the early diagnosis of HIV, the concentration of HIV RNA in the HIV-infected patient samples usually ranges only from 10^2 to 10^6 copies/mL (Avettand-Fènoël et al. 2009; Sivapalasingam et al. 2007). Thus, only one of several thousand or even million picoliter-scale droplets will contain one copy of the target molecule. Larger droplets (nano- to microliter) have to be employed in these cases to increase the chances of detecting the infectious agent. In all cases, though, an understanding of the performance of droplet-based PCR is necessary to properly design and operate such microfluidic systems.

In this paper, we have performed PCR in the aqueous-in-oil droplets generated using sequential injection mode in a microfluidic device with on-chip heating and temperature control. The on-chip electronics allows rapid transition between temperature points and accurate detection of reaction conditions. Unlike the previous studies that are focused on demonstrating a droplet-based microsystem for PCR, we have also provided in-depth studies of the performance of droplet-based PCR by investigating the effect of reaction parameters, including polymerase concentration, Mg^{2+} concentration, hold time at each temperature step, template DNA concentration and droplet size. With the optimized reaction parameters, our system demonstrates the capability of monitoring the amplification in real time and providing faster detection than the benchtop instruments. Our characterization studies will

also aid in the design and operation of similar droplet-based microsystems for use in portable point-of-care diagnosis.

2 Materials and Methods

2.1 Device fabrication

The fluid network is fabricated on a glass wafer using photolithography and wet chemical etching. The detailed procedure have been outlined elsewhere (Pal et al. 2005). Briefly, a thin metal film (500Å Cr/ 2500Å Au) is deposited and patterned on the glass wafer. The glass wafer is then etched to the desired depth in hydrofluoric acid (49%) (CMOS grade; J.T. Baker, Philipsburg, NJ). Next, the photoresist is striped and the metal layer is removed. The glass wafer is then diced to obtain individual dies. The heaters and resistance temperature detectors (RTDs) are fabricated on a silicon wafer with a 5000Å thick silicon oxide layer. Firstly, photoresist is patterned on the silicon wafer using photolithography. Next, 700Å Chromium and 450Å gold are evaporated on the silicon wafer. The wafer is then left in acetone (CMOS grade; J.T. Baker, Philipsburg, NJ) to liftoff unwanted metal. The diced individual silicon dies are fixed on the custom designed printed circuit board (PCB, Advanced Circuits, Aurora, CO), and then wire bonded (Kulicke & Soffa 4124 Ball Bonder) using 1.0 mil gold wire. Finally, the silicon and glass components are visually aligned and then bonded using UV curable optical glue.

2.2 Instrumentation

The setup for reaction temperature control consists of a DC power supply (B+K Precision Model 1760, Yorba Linda, CA), two data acquisition (DAQ) boards (National instruments PCI 6031E and PCI-6704, Austin, TX), two connector blocks (National instruments SCB-100 and SCB-68, Austin, TX), a signal conditioning circuit, a computer and two LabVIEW programs (National instruments, Austin, TX). The RTDs are calibrated by heating the device in a convection oven and recording the temperature-resistance data in a LabVIEW program. The slope and intercept from a linear fit of the temperature and resistance data are read into the control algorithms that use a proportional-integral (PI) module to control temperature. The precision of temperature control is ± 0.2°C. The heaters are connected to the power supply through the signal conditioning circuit that boosts the supply voltage from the computer with an op-amp gain of 3. During the experiments, the device is placed on a copper block that sits on a probe station with temperature maintained at 10°C.

Lab air supply controlled by a regulator (VSO-EP; Parker, Cleveland, OH) provides the pneumatic pressure used to form the droplet in the microdevice. Pressure or vacuum is applied through syringes connected to each port on the device. The Pulsing of pressure or vacuum is controlled by a set of three-way solenoid valves (Numatech, Wixom, MI). Opening and closing of the solenoid valves are operated through a combination of a DC power supply (Electro Industries, Model Digi 35A) and a relay board (Model ER-16; National Instruments, Austin, TX). Functioning of the relay board is controlled through a LabVIEW program and a Digital I/O card (National Instrument PCI-DIO-96, Austin, TX).

2.3 PCR amplification

The PCR mixture consists of λDNA template (Invitrogen, Carlsbad, CA) with the concentration ranging from 3.5ng/μL to 3.5×10^{-4}ng/μL, dNTPs (0.2mM each dATP, dGTP, dCTP and 0.4mM dUTP), 10mM Tris-HCl (pH 8.3), 50mM KCl, 0.01mM EDTA, 3.5mM $MgCl_2$, 0.9μM each primer, 0.25μM probe, 0.01units/μL AmpErase UNG, and 0.175units/μL AmpliTaq Gold® DNA polymerase (Applied Biosystems, Foster City, CA). The sequences of forward and reverse primers are 5’-CATCAAAGCCATGAACAAAGCA-3’

and 5'-TCAGCAACCCCGGTATCAG-3', respectively. The sequence of probe is 5'6FAM-CCGCGCTGGATGA-3'MGBNFQA. This size of the target product is 56bp. The thermocycling protocol used in most of the on-chip droplet-based PCR consists of 50°C for 2min, 95°C for 10min, followed by 16 cycles of 95°C for 9s and 60°C for 30s. PCR grade mineral oil (Sigma Aldrich, St. Louis, MO) is used as the continuous oil phase.

2.4 Fluorescence detection and analysis

An inverted fluorescence microscope (Nikon Eclipse TE2000-U) with a 2× objective (Nikon) is used to monitor fluorescence of the reaction droplet. An X-cite Series 120 lamp (EXFO Life Science Divisions, Ontario, Canada) with FITC filter is used as the excitation source. The fluorescence images are captured using a digital CCD camera (Photometrics Cascade 512F; Roper Scientific, Tucson AZ) with a 500ms exposure time. The relative fluorescence intensity is used to quantify the amplification yield in the droplet, which is calculated by scaling the fluorescence intensity of the droplet by that of the reference area on the device. Data analysis is done by Meta Vue Software.

3 Results and Discussions

3.1 PCR in single submicroliter droplet

Single droplets with a volume range of ~5–250nL were formed reproducibly in a microfabricated device. The device design includes a 45-degree junction followed by a neck region (220μm wide and 60μm long) between the junction and the main channel (400μm wide and 3mm long) (Figure 1(a)). The reaction chamber downstream of the main channel is 1mm wide and 2.5mm long, and the entire fluid network is 100μm deep. A sequential injection mode is employed to form single large droplets (Figure 1(b)–(e)) by first filling the device with mineral oil using capillary forces and then injecting the aqueous reaction solution into the device using pulsed pressure (~4 psig, on for 15 ms, off for 1 sec). The pulsing is turned off once the oil/aqueous interface reaches the desired position in the main channel or the reaction chamber. Next, pulsed pressure (~4 psig, on for 15 ms, off for 1 sec) is applied through the oil inlet to break the aqueous stream in the neck region and then push the droplet into the reaction chamber while simultaneously pushing the rest of the aqueous solution back to the reservoir.

The droplet size is dependent on the position of the oil/aqueous interface in the direction toward the outlet and can easily be controlled by adjusting the strength and frequency of the pulsed pressure. The pressure is applied to individual liquid phases sequentially and thus no balance of the flow rates is necessary. The droplet size is also quite reproducible. For example, when forming 20 droplets with a designed size of 150nL, the average of the actual droplet size is 149.92nL with a standard deviation of 8.45nL. The entire procedure for forming droplets of various sizes (~5–250nL; Figure 1(f)–(k)) takes less than 10 sec.

PCR of λDNA has been successfully performed in the droplets using on-chip metal heaters and RTDs (Figure 1(a)). With FRET probes included in the reaction mixture, the amplification can be detected *in situ* using fluorescent microscopy. As shown in Figure 2, the relative fluorescence intensity of the reaction droplet increases significantly (from 1.007 to 1.464) after 40 cycles of PCR. No volume loss of the reaction solution has been observed as measured using the droplet area in the fluorescent images. This result reveals that the droplet-based microsystem can effectively prevent evaporation during high temperature reactions by encapsulating the reaction solution into the continuous oil phase, eliminating the need for mechanical microvalves.

3.2 Effect of reaction parameters on performance of droplet-based PCR

For a multi-component reaction such as PCR, many parameters can affect the reaction performance. The effect of different parameters should be relatively independent of the droplet size, although some surface-related phenomena may include some size dependence. Therefore, we have studied the effect of a series of reaction parameters including droplet size on PCR performance.

3.2.1 Reagent concentration—Polymerase is a critical reagent that is responsible for catalyzing the PCR amplification. The result in Figure 3 shows that higher polymerase concentration is required for the droplet-based PCR to achieve on-chip amplification comparable to benchtop results. The optimum polymerase concentration is 0.175 U/μL for on-chip droplet PCR, while the recommended concentration for benchtop PCR is 0.025 U/μL. This observation indicates polymerase loss from the aqueous phase, similar to the effect reported for PCR in a single-phase microsystem (Erill et al. 2003;Krishnan et al. 2004). This polymerase loss could be due to the partition of the polymerase to the aqueous/oil interface which reduces the aqueous/oil interfacial tension (Beverung et al. 1999). The polymerase could also be non-specifically adsorbed to the device surface since previous studies have found that *Taq* polymerase has a high adsorption affinity to most surfaces (Prakash et al. 2008).

The Mg^{2+} concentration in the PCR droplet was also varied to determine its effect on the amplification yield. Previous benchtop studies have shown that polymerase can only work with the presence of free Mg^{2+}, but that free Mg^{2+} can also bind to other reaction components such as dNTPs, primers and DNA. As shown in Figure 4, the optimum Mg^{2+} concentration for on-chip droplet-based PCR is 3.5mM, the same as that in the benchtop PCR and the single-phase on-chip PCR (Krishnan et al. 2004). A higher (5.5mM) or lower (1.5mM) Mg^{2+} concentration results in significantly lower fluorescence intensity of reaction droplet, indicating the inhibition of amplification. However, in benchtop PCR the amplification efficiency is relatively insensitive to Mg^{2+} concentration within the range of 3.5–5.5mM (data not shown). One possible explanation to the different effects of high Mg^{2+} concentration on benchtop and droplet-based PCR might be that as divalent cation, Mg^{2+} could bind to the O^- group on the chamber surface (Voorthuyzen et al. 1987) of the microdevice and function as an ion bridge between the chamber surface and the negatively charged DNA, which reduces the free template DNA in the reaction mixture. When the Mg^{2+} concentration increases (> 3.5mM), the “DNA loss” could become more drastic due to the high surface-to-volume ratio of the microdevice, resulting in the decrease of PCR yield.

3.2.2 Hold time at each temperature step—Rapid heat transfer in microfludic devices allows droplet-based PCR to achieve comparable efficiencies to the benchtop amplification with less reaction time. However, the hold time at each temperature step still needs to be optimized to ensure that the droplet reaches and maintains the desired temperature for a sufficient time required by the reaction kinetics. In addition, unlike the single-phase based microsystem where the reaction solution is isolated by air, the PCR droplet is surrounded by oil that has higher thermal conductivity and thermal mass than air. Therefore, it may take a longer time for the reaction solution in the droplet to reach the desired temperature than that in the single-phase based microdevice.

Figure 5 shows the effect of hold time at each PCR step (activation, denaturation, and annealing/extension) on the amplification yield. The optimum thermal activation time is 10 min, while shorter or longer activation suppresses the reaction (Figure 5(a)). As shown in Figure 5(b), the fluorescence intensity of reaction droplet increases with the increase of denaturation time, and reaches a maximum value at about 9 sec. Moreover, the PCR yield

will not be improved by further extending the denaturation time. At the annealing/extension step, the fluorescence intensity and the hold time show a relationship similar to that at the denaturation step (Figure 5(c)), with an optimum hold time of 30 sec. Although a hold time of 40 sec for annealing and extension further increases the amplification yield, 30 sec was chosen as the optimum hold time considering the tradeoff between the hold time and the reaction yield. Using the optimized hold time at each temperature, the total reaction time for on-chip droplet PCR is half of that for benchtop PCR. With the current system, the heating and cooling rate is 9°C/s and 3.5°C/s, respectively. Although it is possible to further accelerate the temperature transition by optimizing the heater design and achieving better local heating using thermal isolation techniques, the total reaction time may not be reduced since it is mainly limited by the reaction kinetics.

3.2.3 Template DNA quantity—PCR with different amounts of template (λDNA) have been performed using the optimized reaction parameters. The quantity of template DNA in the droplet is determined by the template concentration and the droplet size. As shown in Figure 6, the fluorescence intensity of the reaction droplet increases with increasing template DNA concentration. Also, for a given template concentration, larger droplets give higher fluorescence intensity (Figure 7(a)). Results in both Figure 6 and 7(a) indicate that, overall, there is a positive effect of template DNA quantity on the PCR yield. In addition, with the same quantity of template DNA (10^6 to 10^7 copies), the fluorescence intensity in the reactions with fixed droplet size is approximately the same as that in the reactions with fixed template DNA concentration.

However, there is no clear trend for the relationship between the amplification yield (*i.e.*, fluorescence intensity) and the droplet size. Presumably, if adsorption of reagents on either the chamber walls or the liquid-liquid interface was occurring, reaction performance would decrease as the surface-to-volume ratio (S/V) increased. Figure 7(b) indicates the total S/V (S_T/V) as well as the contribution from the walls (S_W/V) and the interface (S_i/V). The fluorescence intensity is relatively constant in droplets smaller than 80nL (Figure 7(a)) even though in this region the S_i/V and S_T/V dramatically increase with decreasing droplet size (Figure 7(b)). However, since these droplets are disc-shaped (confined by the top and bottom chamber walls but free from the side walls), the wall surface-to-volume ratio (S_W/V) is relatively constant. These results suggest the adsorption to the chamber surface is more important than adsorption to the liquid interface. Note that, when droplets are larger than 80nL, the S_i/V and S_T/V still increase with decreasing drop size albeit at a lower rate. The apparent decrease in fluorescence intensity with decreasing droplet size may thus be explained by adsorption onto the chamber solid surfaces, but more studies need to be conducted to confirm this effect.

3.3 Droplet-based real-time amplification

A series of PCR with template concentration from 6.69×10^3 copies/μL to 6.69×10^7 copies/μL have been performed. The real-time fluorescence intensity of the reaction droplet is plotted in Figure 8. The trendline of intensity data at each template concentration exhibits a typical amplification profile including an exponential, linear and plateau phase. Moreover, higher template DNA concentrations correspond to an earlier start point of the detectable increase in the fluorescence intensity of the reaction droplet. With a threshold value of fluorescence intensity equal to 1.13 (*i.e.*, the value at which the fluorescence intensity starts increasing above the background signal), the cycle threshold (Ct) is determined using interpolation in Figure 8 and plotted in Figure 9. The linear relationship between the template DNA concentration and Ct indicates the potential application of quantitative PCR using submicroliter droplets.

The data with the same template concentration range collected on a benchtop real-time PCR instrument are also plotted in Figure 9, in order to compare the performance of the benchtop and droplet-based systems. As shown in Figure 9(a), the cycle thresholds obtained in the droplet-based PCR are approximately the same as those generated in the benchtop reactions with the same template DNA concentration. But with the same template DNA copy number, the cycle thresholds obtained in the droplet-based PCR are ~10 cycles earlier than those generated in the benchtop reactions (Figure 9(b)), which indicates a faster analysis using our microsystem.

4 Conclusions

We have successfully performed PCR in on-chip generated single nanoliter sized droplets with on-chip heating and temperature control. Without any microvalves or on-chip sealing components, no volume loss of the reaction droplet has been observed after 40 cycles of PCR. Most importantly, our study adds to previous studies that specifically addressed the dependence of droplet-based PCR amplification efficiency on many of the reaction parameters including reagent concentration, hold time at each temperature step and droplet size. These studies not only provide detailed information on the behavior of this well-characterized bioreaction in a small-scale droplet-based system, but also will aid in optimizing the design and operation of the microfluidic systems. With the optimized reaction parameters, our device demonstrates the sensitivity of detecting the template DNA concentration within a wide concentration range, and the capability of rapid detection using this droplet-based system for real-time quantitative PCR.

Acknowledgments

The authors would like to gratefully acknowledge the funding of this work through the grants (5-R01-AI049541-06 and 1-R01-EB006789-01A2) from the National Institutes of Health. The authors would like to acknowledge Brian N. Johnson, Dustin Chang and Abhishek Shetty for their assistance with reagent preparation, device fabrication, lab maintenances and general discussions.

References

Ahmed R, Jones TB. J. Electrost. 2006; 64:543–549.

Anna SL, Bontoux N, Stone HA. Appl. Phys. Lett. 2003; 82:364–366.

Avettand-Fènoël V, Chaix M-L, Blanche S, Burgard M, Floch C, Toure K, Allemon M-C, Warszawski J, Rouzioux C. J. Med. Virol. 2009; 81:217–223. [PubMed: 19107966]

Beer NR, Hindson BJ, Wheeler EK, Hall SB, Rose KA, Kennedy IM, Colston BW. Anal. Chem. 2007; 79:8471–8475. [PubMed: 17929880]

Beer NR, Wheeler EK, Lee-Houghton L, Watkins N, Nasarabadi S, Hebert N, Leung P, Arnold DW, Bailey CG, Colston BW. Anal. Chem. 2008; 80:1854–1858. [PubMed: 18278951]

Beverung CJ, Radke CJ, Blanch HW. Biophys, Chem. 1999; 81:59–80. [PubMed: 10520251]

Bringer MR, Gerdts CJ, Song H, Tice JD, Ismagilov RF. Phil. Trans. R. Soc. Lond. A. 2004; 362:1087–1104.

Burns MA. Science. 2002; 296:1818–1819. [PubMed: 12052944]

Chabert M, Dorfman KD, de Cremous P, Roeeraade J, Viovy J-L. Anal. Chem. 2006; 78:7722–7728. [PubMed: 17105164]

Chabert M, Viovy J-L. Proc. Natl. Acad. Sci. 2008; 105:3191–3196. [PubMed: 18316742]

Chan EM, Alivisatos AP, Mathies RA. J. Am. Chem. SOC. 2005; 127:13854–13861. [PubMed: 16201806]

Chen C-T, Lee G-B. J. Micorelectromech. Syst. 2006; 15:1492–1498.

Cho SK, Moon H, Kim C-J. J. Microelectromech. Syst. 2003; 12:70–80.

Dittrich PS, Jahnz M, Schwille P. ChemBioChem. 2005; 6:811–814. [PubMed: 15827950]

Erill I, Campoy S, Erill N, Barbé J, Aguiló J. Sens. Acutators. B. 2003; 96:685–692.

Garstecki P, Fuerstman MJ, Stone HA, Whitesides GM. Lab Chip. 2006; 6:437–446. [PubMed: 16511628]

Guttenberg Z, Müller H, Habermüller H, Geisbauer A, Pipper J, Felbel J, Kielpinski M, Scriba J, Wixforth A. Lab Chip. 2005; 5:308–317. [PubMed: 15726207]

He M, Edgar JS, Jeffries GDM, Lorenz RM, Shelby JP, Chiu DT. Anal. Chem. 2005; 77:1539–1544. [PubMed: 15762555]

Hsiung S-K, Chen C-T, Lee G-B. J. Micromech. Microeng. 2006; 16:2403–2410.

Huebner A, Srisa-Art M, Holt D, Abell C, Hollfelder F, deMello AJ, Edel JB. Chem. Commun. 2007:1218–1220.

Hung L-H, Choi KM, Tseng W-Y, Tan Y-C, Shea KJ, Lee AP. Lab Chip. 2006; 6:174–178. [PubMed: 16450024]

Jones TB. J. Electrost. 2001; 51–52:290–299.

Krishnan M, Burke DT, Burns MA. Anal. Chem. 2004; 76:6588–6593. [PubMed: 15538781]

Kumaresan P, Yang CJ, Cronier SA, Blazej RG, Mathies RA. Anal. Chem. 2008; 80:3522–3529. [PubMed: 18410131]

Lehmann U, Vandevyver C, Parashar VK, Gijs MAM. Angew. Chem. Int. Ed. 2006; 45:3062–3067.

Link DR, Anna SL, Weitz DA, Stone HA. Phys. Rev. Lett. 2004; 92:054503-1–054503-4. [PubMed: 14995311]

Link DR, Grasland-Mongrain E, Duri A, Sarrazin F, Cheng Z, Cristobal G, Marquez M, Weitz DA. Angew. Chem. Int. Ed. 2006; 45:2556–2560.

Mohr S, Zhang Y-H, Macaskill A, Day PJR, Barber RW, Goddard NJ, Emerson DR, Fielden PR. Microfluid Nanofluid. 2007; 3:611–621.

Nisisako T, Torii T, Higuchi T. Lab Chip. 2002; 1:24–26. [PubMed: 15100856]

Niu X, Gulati S, Edel JB, deMello AJ. Lab Chip. 2008; 8:1837–1841. [PubMed: 18941682]

Ohashi T, Kuyama H, Hanafusa N, Togawa Y. Biomed Microdevices. 2007; 9:695–702. [PubMed: 17505884]

Pal R, Yang M, Lin R, Johnson BN, Srivastava N, Razzacki SZ, Chomistek KJ, Heldsinger D, Haque RM, Ugaz VM, Thwar P, Chen Z, Alfano K, Yim M, Krishnan M, Fuller AO, Larson RG, Burke DT, Burns MA. Lab Chip. 2005; 5:1024–1032. [PubMed: 16175256]

Pipper J, Inoue M, Ng LF-P, Neuzil P, Zhang Y, Novak L. Nat. Med. 2007; 13:1259–1263. [PubMed: 17891145]

Pollack MG, Fair RB, Shenderov AD. Appl. Phys. Lett. 2000; 77:1725–1726.

Pollack MG, Shenderov AD, Fair RB. Lab Chip. 2002; 2:96–101. [PubMed: 15100841]

Prakash AR, Amrein M, Kaler KVIS. Microfluid. Nanofluid. 2008; 4:295–305.

Sarrazin F, Prat L, Miceli ND, Cristobal G, Link DR, Weitiz DA. Chem. Eng. Sci. 2007; 62:1042–1048.

Shestopalov I, Tice JD, Ismagilov RF. Lab Chip. 2004; 4:316–321. [PubMed: 15269797]

Sivapalasingam S, Patel U, Itri V, Laverty M, Mandaliya K, Valentine F, Essajee S, Trop J. Pediatrics. 2007; 53:355–358.

Song H, Bringer MR, Tice JD, Gerdts CJ. Appl. Phys. Lett. 2003; 83:4664–4666. [PubMed: 17940580]

Srinivasan V, Pamula VK, Fair RB. Lab Chip. 2004; 4:310–315. [PubMed: 15269796]

Srisa-Art M, deMello AJ, Edel JB. Anal. Chem. 2007; 79:6682–6689. [PubMed: 17676925]

Tan Y-C, Fisher JS, Lee AL, Cristini V, Lee AP. Lab Chip. 2004; 4:292–298. [PubMed: 15269794]

Thorsen T, Roberts RW, Arnold FH, Quake SR. Phys. Rev. Lett. 2001; 86:4163–4166. [PubMed: 11328121]

Ting TH, Yap YF, Nguyen N-T, Wong TN, Chai JCK, Yobas L. Appl. Phys. Lett. 2006; 89:234101–234103.

Um E, Park J-K. Lab Chip. 2009; 9:207–212. [PubMed: 19107275]

Voorthuyzen JA, Kesin K, Bergveld P. Surf. Sci. 1987; 187:201–211.

Wang F, Yang M, Burns MA. Lab Chip. 2008; 8:88–97. [PubMed: 18094766]
Yang H, Park CC, Hu YT, Leal LG. Phys. Fluids. 2001; 13:1087–1106.
Yobas L, Martens S, Ong W-L, Ranganathan N. Lab Chip. 2006; 6:1073–1079. [PubMed: 16874381]
Zheng B, Tice JD, Roach S, Ismagilov RF. Angew. Chem. Int. Ed. 2004; 43:2508–2511.

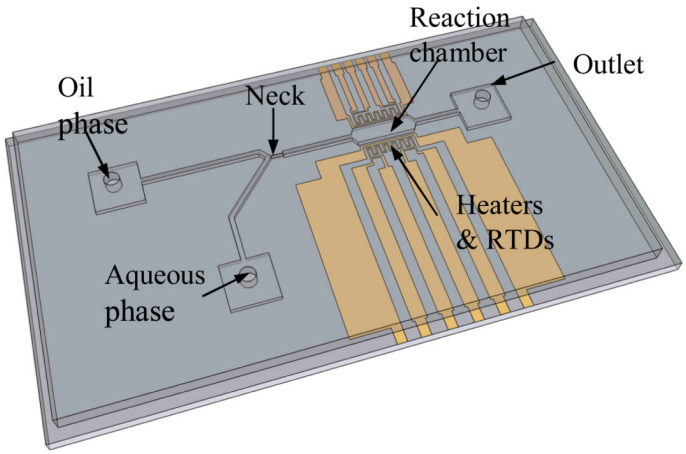

(a)

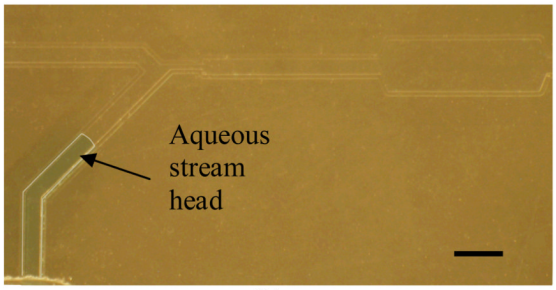

(b)

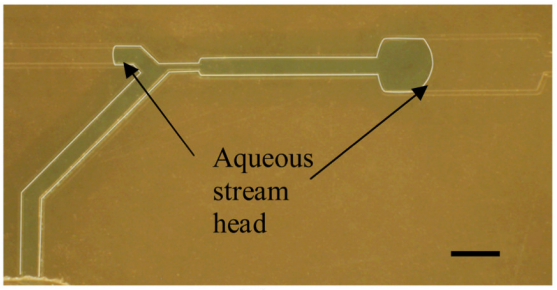

(c)

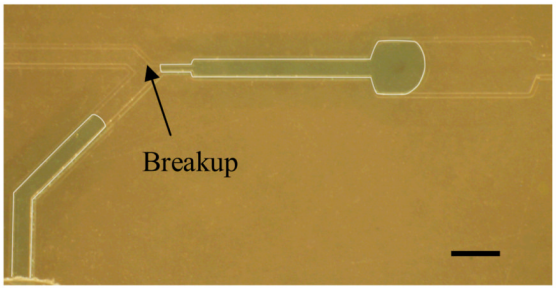

(d)

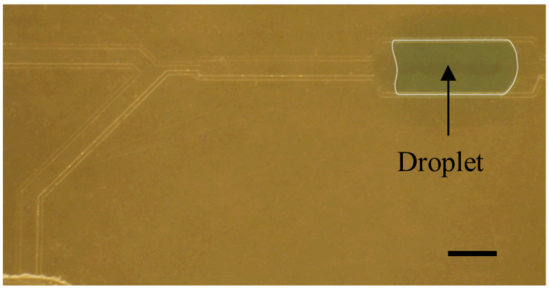

(e)

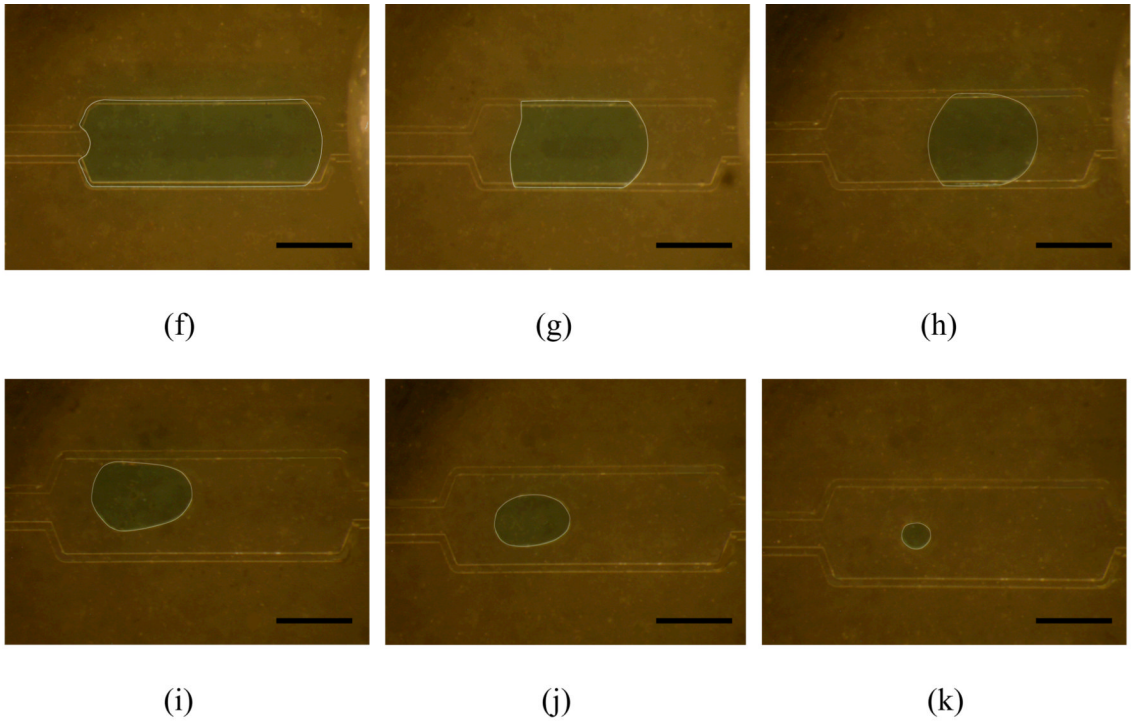

Fig.1.
(a) Schematic of the device design. (b)–(e) Formation process of single submicroliter droplet. (f)–(k) On-chip formed different sized single droplet: (f) ~225nL; (g) ~125nL; (h) ~80nL; (i) ~40nL; (j) ~26nL; (k) ~5nL. All the scale bars represent 800μm.

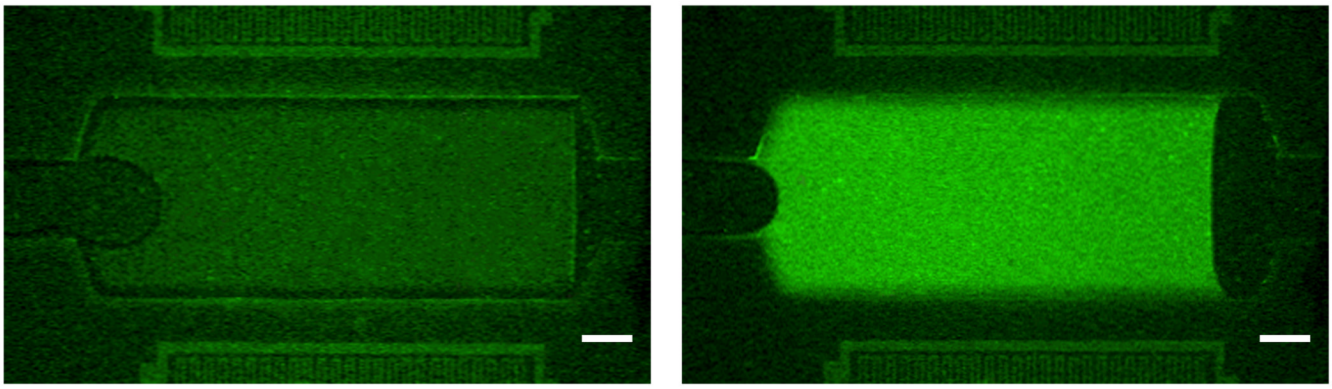

(a) (b)

Fig.2.

Fluorescence images of the reaction droplet (a) before PCR and (b) after 40 PCR cycles. The template λDNA concentration is 3.5ng/μL (~6.69×10^7 copies/μL). The droplet size is ~225nL. The scale bar represents 250μm.

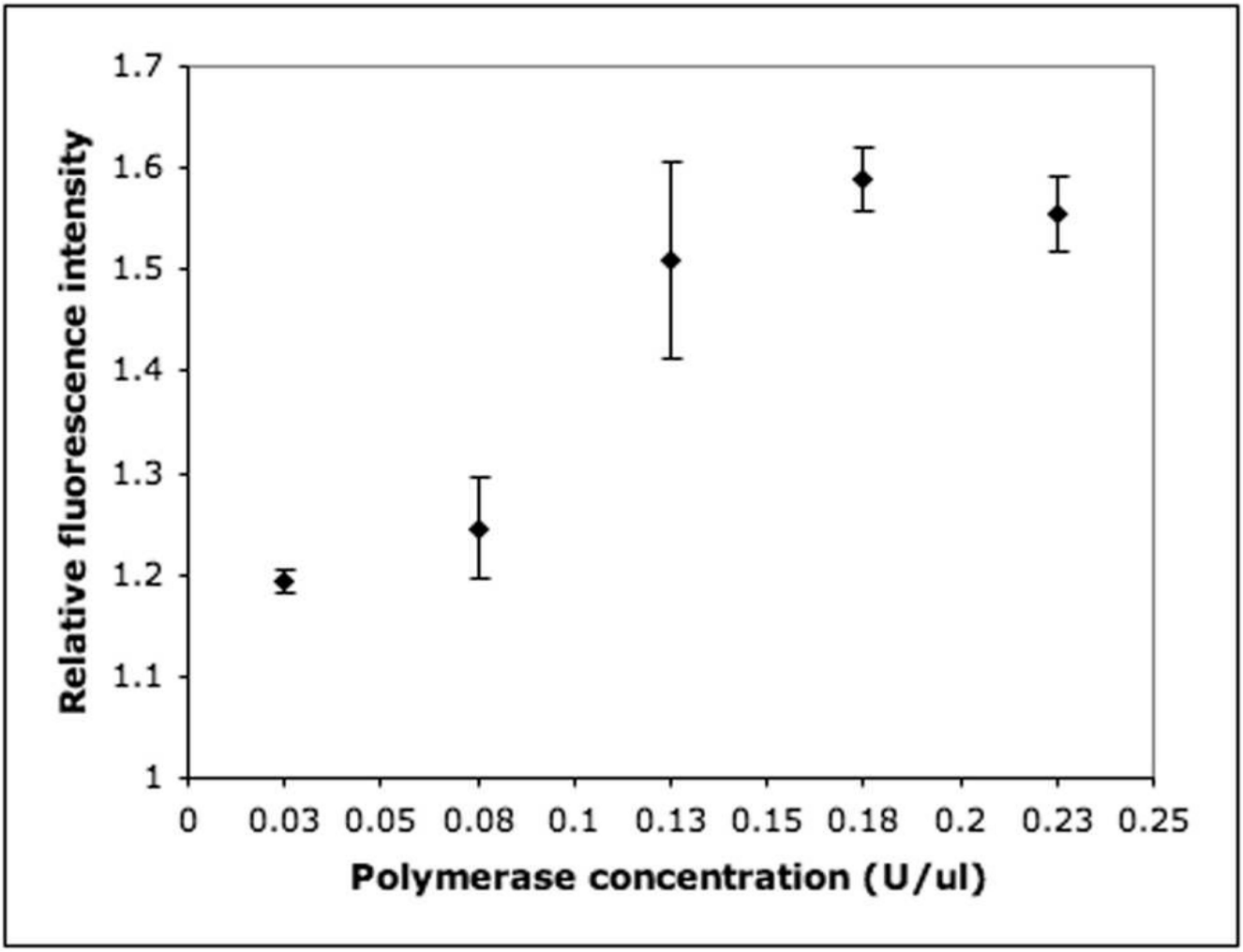

Fig.3.

Effect of polymerase concentration on amplification efficiency. The template λDNA concentration is 3.5ng/μL (~6.69×10^7 copies/μL). The droplet size is ~150nL. The error bar represents the standard deviation.

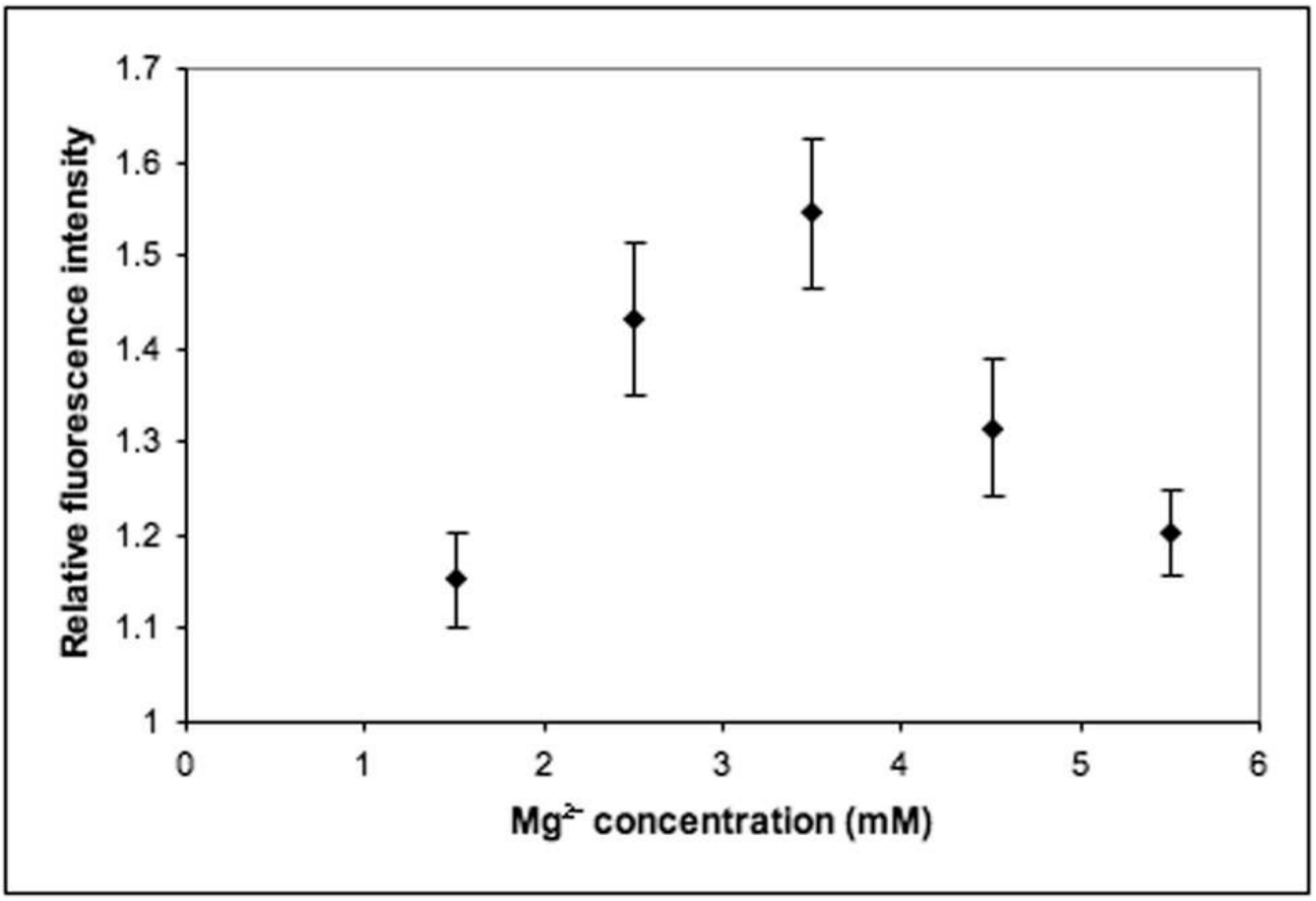

Fig.4.

Effect of Mg^{2+} concentration on amplification efficiency. The template λDNA concentration is 3.5ng/μL (~6.69×10^7 copies/μL). The droplet size is ~150nL. The error bar represents the standard deviation.

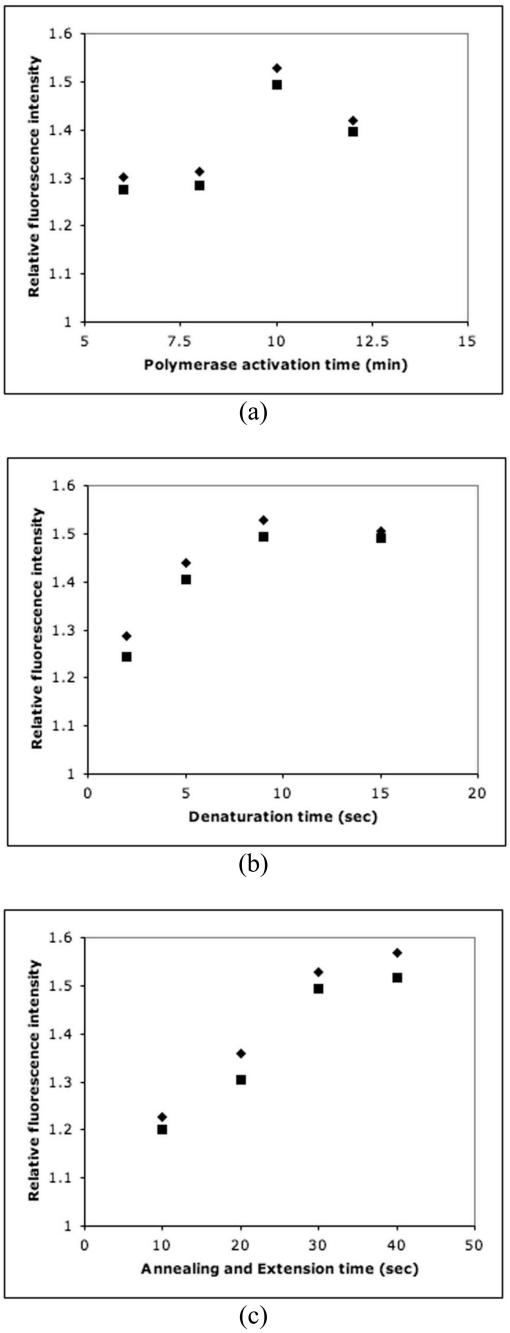

Fig.5.

Effect of hold time at different temperature step on amplification efficiency. (a) Thermal activation step; (b) denaturation step; (c) annealing/extension step. The template λDNA concentration is 3.5ng/μL. The droplet size is ~150nL. The data are from duplicate experiments.

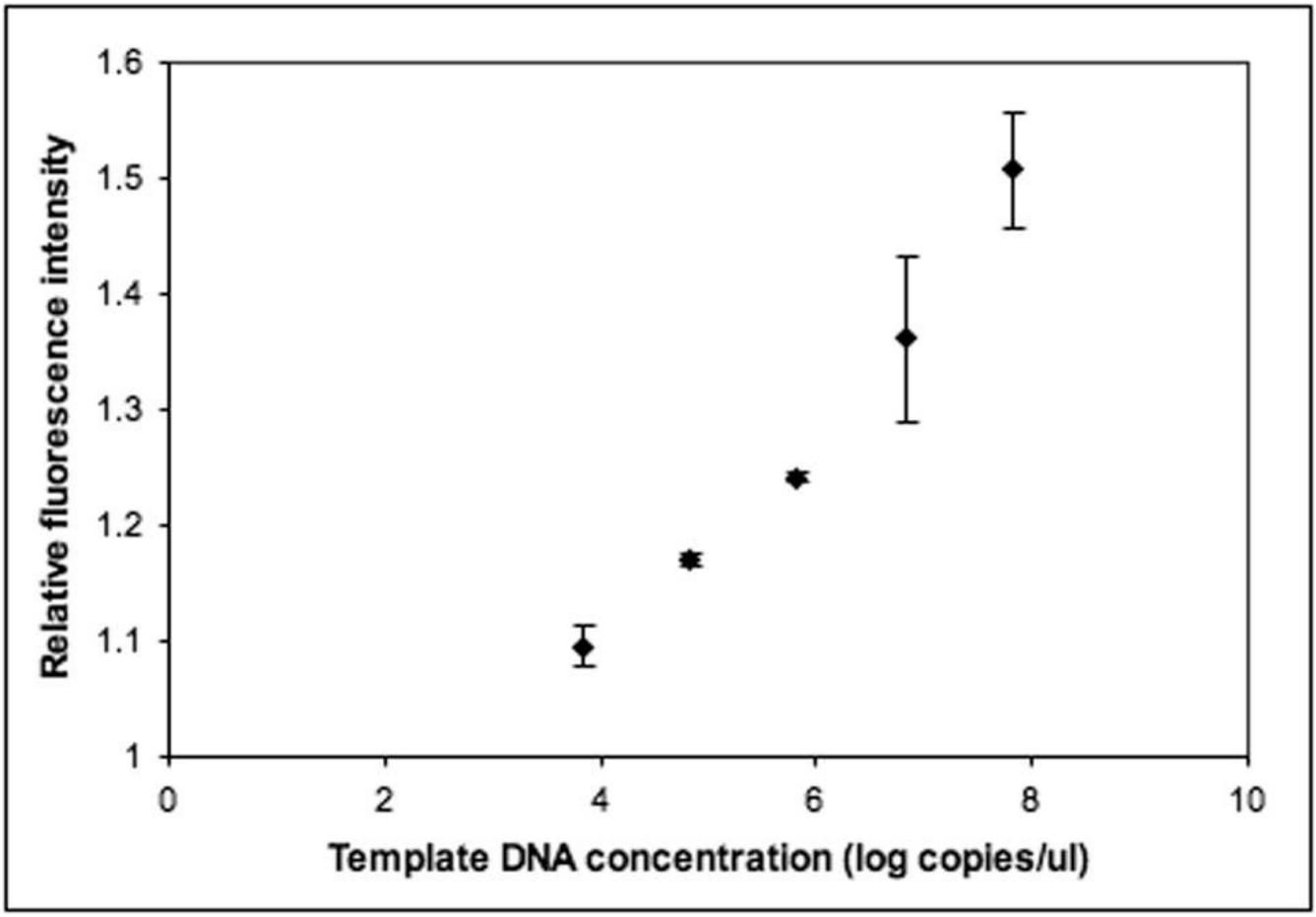

Fig.6.
Fluorescence intensity of reaction droplet containing different concentrations of template λDNA after 16 PCR cycles. The droplet size is ~150nL. The error bar represents the standard deviation.

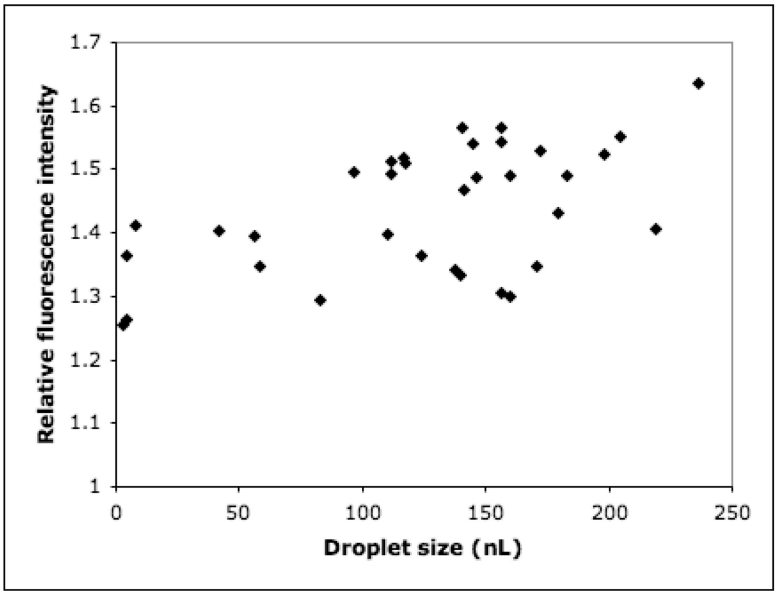

(a)

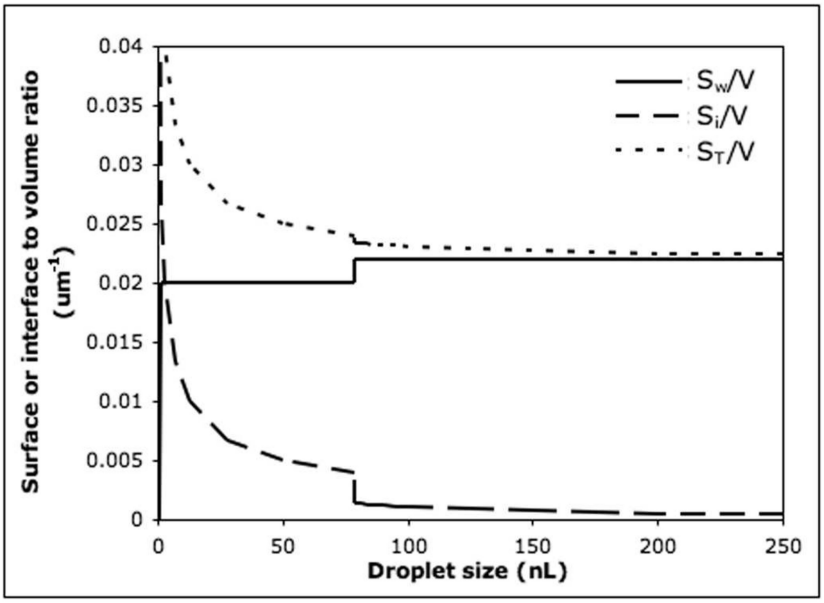

(b)

Fig.7.

(a) Fluorescence intensity of different sized reaction droplet after 16 PCR cycles. The template DNA concentration is 3.5ng/μL (~6.69×10^7 copies/μL) in all the droplets. (b) Calculated surface to volume ratio of different sized droplets. V is the droplet volume; S_w is the area of the droplet surface confined by the chamber walls; S_i is the area of the unconfined liquid-liquid interface of the droplet; S_T is the total surface area of the droplet. The step in the curves indicates when the droplets become from disc-shaped (< 80μL) to plug-shaped (> 80μL).

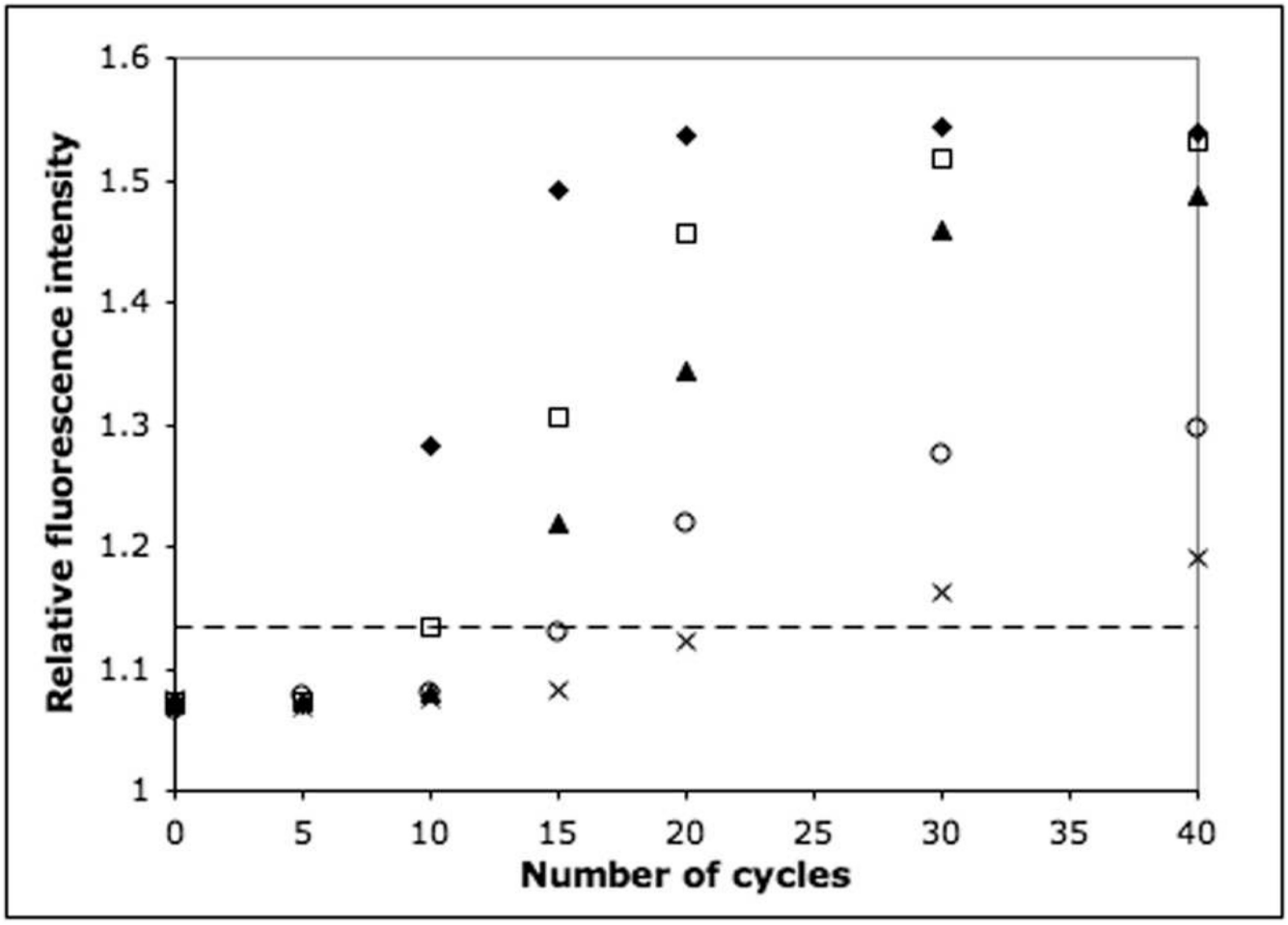

Fig.8.

Real-time fluorescence intensity of reaction droplet with different template concentration. ◆ 3.5ng/μL (~6.69×10^{7} copies/μL) of template λDNA; □ 0.35ng/μL (~6.69×10^{6} copies/μL) of template λDNA; ▲ 0.035ng/μL (~6.69×10^{5} copies/μL) of template λDNA; ○ 3.5×10^{-3} ng/μL (~6.69×10^{4} copies/μL) of template λDNA; × 3.5×10^{-4} ng/μL (~6.69×10^{3} copies/μL) of template λDNA. The droplet size for all different template concentrations is ~150nL.

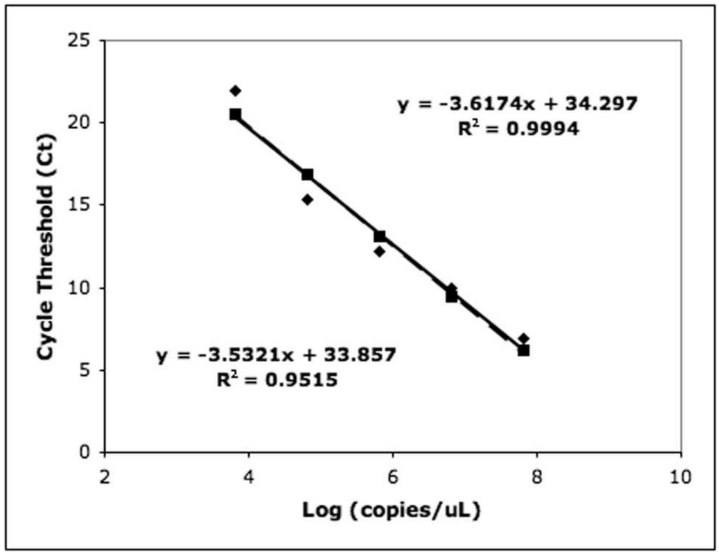

(a)

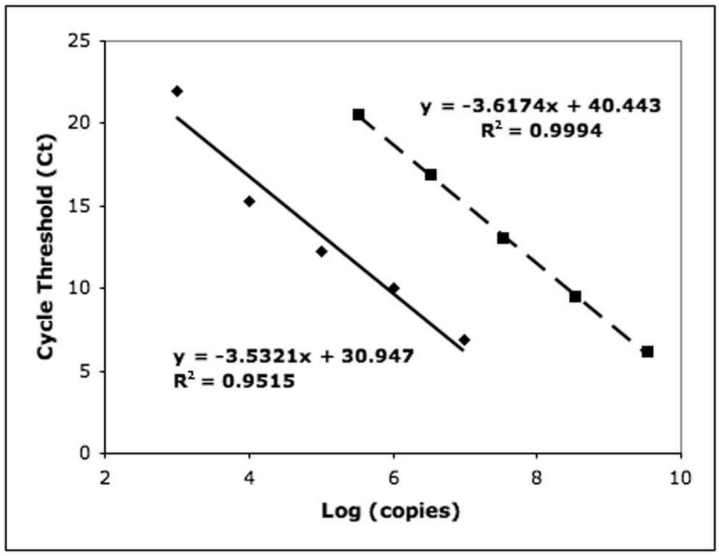

(b)

Fig.9.

(a) Cycle threshold versus logarithm of template DNA concentration (copies/μL). (b) Cycle threshold versus logarithm of template DNA copy number. In both (a) and (b), ◆ denotes the data obtained using the microdevice, and ■ denotes the data generated on a benchtop instrument; the equation in the top right is for the trendline (dash line) of the benchtop data, and the equation in the bottom left is for the trendline (solid line) of the on-chip data. The benchtop reaction volume is 50μL.